

First-principles study the structural, magnetic, optical properties and doping effect in chromium arsenide

Na Kang,¹ Wenhui Wan,^{1, a)} Bu-Sheng Wang,¹ Kai-Cheng Zhang,² and Yong Liu^{1, b)}

¹⁾State Key Laboratory of Metastable Materials Science and Technology & Key Laboratory for Microstructural Material Physics of Hebei Province, School of Science, Yanshan University, Qinhuangdao, 066004, People's Republic

²⁾College of Mathematics and Physics, Bohai University, Jinzhou 121013, China

We systematically study the pristine and doped chromium arsenide in various crystal structures to investigate the structural, magnetic, and optical properties for real applications. By first-principles calculations, we show the structural parameters, the ground magnetic state, density of states, and the optical properties of CrAs in six different structures. The results regarding structural parameters and magnetic properties agree well with experimental data and other theoretical works. First, We found that the ground-state structure is an orthorhombic MnP-type structure with antiferromagnetic spin order. The rocksalt structure is an unreported metastable phase and a ferromagnetic metal with high spin polarization at the Fermi level. Secondly, the NiAs structure and MnP structure have a higher absorption coefficient than other structures in the infrared region and ultraviolet region, respectively. In the visible light region, the wurtzite and zincblende structures are more transparent than other structures. At last, we found that Ti substitution of Cr and Te substitution of As can lead to a phase transition in ground-state structure and ground-state magnetic order, respectively. These results can promote the application of the CrAs system into spintronics.

PACS numbers: 71.20.-b, 78.20.Bh, 78.20.Ci, 71.55.-i

I. INTRODUCTION

Spintronics (or magnetoelectronics)¹, which adds the spin degree of freedom to the conventional electronic devices, has several advantages like increasing data processing, decreased electric power consumption, and non-volatility²⁻⁴. In 1983, de Groot *et al* predicted half Heusler alloys NiMnSb and PtMnSb⁵ to be Half-metallic (HM) materials, which have 100% spin polarization at Fermi level. Transition metal pnictides (e.g. CrAs and VAs) have various phases including zincblende (ZB), wurtzite (WZ), hexagonal NiAs (NA), and orthogonal MnP (MP)-type structures⁶. These materials have rich magnetic orders and compatibility with the traditional group III-V or II-VI semiconductors (e.g. GaAs, ZnTe)⁶. Thus, it is significant to explore the electric and magnetic properties of transition metal pnictides⁷.

Chromium arsenide (CrAs) exhibit an MP-type orthorhombic structure at low temperature^{8,9}. T. Ito *et al* predicted that MP-type CrAs shows a double-spiral antiferromagnetic (AFM) magnetic order with the magnetic moment of $1.7 \mu_B$ per Cr atom¹⁰. Kotegawa *et al* observed a first-order antiferromagnetic-paramagnetic transition at 265 K, which is interpreted as an electronic transition between localized and collective states¹¹. Svitlana Polesya *et al* proved that nearest-neighbor and next nearest-neighbor Cr-Cr interactions in CrAs are ferromagnetic (FM) and AFM, respectively, which can give the magnetic phase transition temperature is about 270 K¹², consistent with the experiment value¹³. Wu *et al.*¹⁴

and Kotegawa *et al*¹⁵ independently discovered pressure-induced unconventional superconductivity in the vicinity of antiferromagnetic (AFM) order in MP-type crystal structure CrAs. Carmine *et al* predicted that CrAs may be a weakly correlated material with the Fermi surface exhibiting a two-dimensional behavior, which suggests a close link between the appearance of the superconductivity and the external pressure¹⁶. Moreover, W. Wu *et al* observed that MP-type CrAs show a Fermi-liquid behavior with a T^2 -dependent resistivity at low temperature¹⁷.

Much research effort has also been devoted into other meta-stable phases of CrAs. N. Kazama *et al*¹⁸ observed that CrAs occurs a structural phase transition from the MnP structure to NiAs structure at high $T = 769$ K. Another meta-stable ZB-type CrAs has been fabricated on GaAs(001) substrates by molecular-beam-epitaxy (MBE)^{19,20}. The experiment confirmed that ZB-type CrAs have well-pronounced HM behavior with high Curie temperature above 400 K^{20,21}. Xie *et al*²² predicted WZ-type CrAs to be HM ferromagnet. Besides, the magnetic properties of CrAs are very sensitive to substitutions of other elements. Suzuki and Ido reported that substitution of only 7.5% of phosphorus for arsenic in CrAs yields a collapse of the double-spiral magnetic order²³. Meanwhile, the transition temperature of CrAs is very sensitively influenced by other 3d metal substitutions for the Cr^{24,25}. The previous theoretical research paid little attention to the doping effect on the structural properties as well as the optical properties of CrAs system. It is meaningful to explore the structural, magnetic, optical and electronic structural properties of pristine and doped CrAs in various structures.

Here, we focused on a systematical study of CrAs in various crystal structures utilizing the density functional theory. We performed first-principles calculations

^{a)}Electronic mail: wwh@ysu.edu.cn

^{b)}Electronic mail: yongliu@ysu.edu.cn or ycliu@ysu.edu.cn

based for CrAs in six phases including the Rocksalt (RS), Cesium-chloride (CC), ZB, WZ, NA, and MP phase. Then we displayed their optical properties. At last, we report the doping effect on the structural and magnetic properties of CrAs. The computational details are given in the next section. The main results and discussion will be presented in the third section. We shall give our conclusion in the fourth section.

II. COMPUTATIONAL DETAILS

Our density functional theory(DFT) calculations were performed by using the Vienna ab initio simulation package(VASP)²⁶⁻²⁸. This code solves the Kohn-Sham equations within the pseudopotential approximation²⁹. The generalized gradient approximation(GGA) to the exchange-correlation potential in form of the Perdew, Burke, and Ernzerhof(PBE)³⁰ functional was used in this work. After convergence tests, an energy cutoff of 650 eV for the plane-wave expansion was selected. The K-points, sampling over the irreducible Brillouin zone, were generated by Monkhorst-Pack scheme³¹. We used K-points mesh of $9 \times 9 \times 9$ for RS, CC, ZB; $11 \times 11 \times 7$ for WZ, NA; and $7 \times 11 \times 7$ for MP type, respectively. The convergence of the results concerning k-point sampling has been carefully checked. To explore the magnetic properties of CrAs, we have calculated the total energy of NM, FM, and different AFM phases for six crystal structures. All the structures have been optimized to achieve the minimum energy by accurate relaxation of the atomic positions up to the energy accuracy of 10^{-5} eV. The optical properties of solids are described by dielectric functions^{32,33}.

III. RESULTS AND DISCUSSIONS

A. Structural analysis of six structures

(i) RS-type CrAs has a space group of $Fm\bar{3}m$ (No.225). It composes of two face-centered cubic lattices, shifted by the vector $(0.5, 0.5, 0.5)$, which results in octahedral coordination for both cations and anions.

(ii) C-type CrAs has a space group of $P6_3mc$ (No.221). The CC structure can be described as two interpenetrating simple cubic lattices shifted by the vector $(0.5, 0.5, 0.5)$ along the body diagonal of the conventional cube. Each anion in a given sublattice has 8 nearest neighboring cations on the other sublattice, there are 6 second nearest neighbors of the same type sublattice.

(iii) ZB-type CrAs has a space group $F\bar{4}3m$ (No.216). The ZB structure is similar to that of diamond with two interpenetrating face-centered-cubic lattices displaced by the vector $(0.25, 0.25, 0.25)$ along the body diagonal of the conventional cube. The coordination number is 4 for each atom.

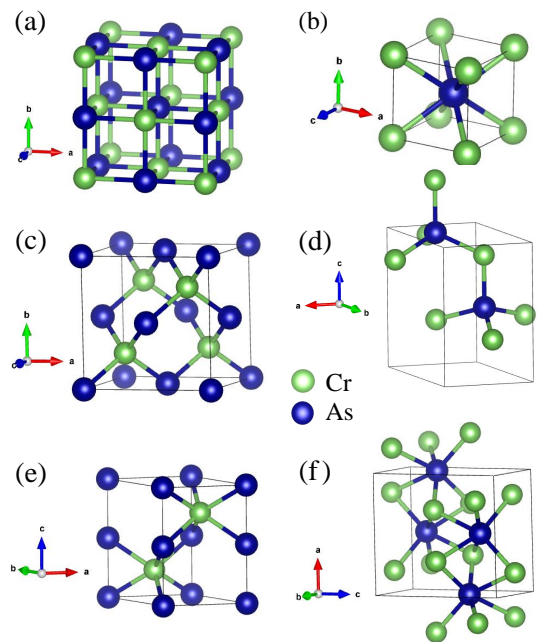


FIG. 1. Six types of crystal structures of CrAs. (a) the cubic Rocksalt (RS) structure; (b) the cubic CsCl (CC) structure; (c) the cubic Zinblende (ZB) structure; (d) the hexagonal Wurtzite-type (WZ) structure; (e) the hexagonal NiAs-type (NA) structure; and (f) the orthorhombic MnP-type structure.

(iv) WZ-type CrAs has a space group $P6_3mc$ (No.186). The WZ structure is regarded as a distorted ZB-type structure with small shifts of atomic positions. There are four atoms of two different types in the unit cell (see Figure 1(d)). Each atom is surrounded by an tetrahedron of atoms of opposite sort hexagonal analog to the ZB structure and has the same local environment if one assumes the ideal c/a ratio and internal parameters u of $3/8$ for the anion site.

(v) NA-type CrAs has a space group $P6_3/mmc$ (No.194), as shown in Figure 1(f). It has four atoms in the primitive unit cell. As atoms form a lattice like the hexagonal close-packed structure, and Cr atoms a simple hexagonal lattice. As distortion and shifts are small, the NA and MP structures are similar. However even the slight difference affects magnetic properties through the change of electronic structure.

(vi) MP-type CrAs has a space group $Pnma$ (No.62). The orthorhombic MnP-type structure is regarded as distorted NiAs-type structure with small shifts of atomic positions³⁸. The structure, illustrated in Figure 1(e), shows that each Cr atom is coordinated to six As atoms in irregular octahedral coordination. Each As atom is surrounded by six Cr atoms, arranged at the corners of a distorted trigonal prism. This structure possesses a space-inversion symmetry.

TABLE I. The lattice types (LT), space group (SG), magnetic state (MS), lattice constant $a(\text{\AA})$, length of Cr-As bond $L(\text{\AA})$, bulk module B (GPa), magnetic moment per formula unit M (μ_B), cohesive energy and per CrAs pair E_c (eV), and relative energy to MP-type structure E_m (eV). The abbreviation TW and OW represent the this work and other work, respectively.

Results	LT	SG	MS	a/b/c	L	B	M	E_c	E_m
TW	MP	62	AFM	5.5705/3.4981/6.2702	2.5562	83.33	-	-7.418	0
OW ⁸	MP	62	AFM	5.5773/3.5731/6.1289	-	-	-	-	-
OW ³⁴	MP	62	AFM	5.637/3.445/6.197	-	-	-	-	-
OW ³⁵	MP	62	NM	5.649/3.465/6.209	-	-	-	-	-
TW	NA	194	AFM	3.7793/5.3234	2.5558	135.36	-	-7.377	0.041
OW ³⁴	NA	194	AFM	3.628/5.561	-	-	-	-	-
OW ³⁶	NA	194	NM	3.55/5.68	-	-	-	-	-
TW	CC	221	FM	3.0003	2.5983	147.62	1.183	-6.792	0.626
TW	WZ	186	FM	4.15/6.71	2.5178	68.65	3.000	-6.533	0.887
OW ²²	WZ	186	FM	4.002/6.530	-	68.4	3.000	-	-
TW	RS	225	FM	5.1205	2.5603	94.86	2.931	-7.026	0.392
TW	ZB	216	FM	5.6683	2.4545	68.83	3.000	-6.533	0.885
OW ³⁷	ZB	216	FM	5.659	-	71.0	3.000	-6.533	-

B. The ground-state and metastable structures

In the fully optimized calculations, all lattice parameters and internal atomic positions were relaxed to find out the ground state of CrAs. By fitting the Birch-Murnaghan equation of state to the obtained total energies as a function of volume, the structural properties of the systems were determined.

We first investigated the NM, FM, and AFM states of CrAs in the MP-type structure. As seen in Figure 2(b), the MP-type CrAs in AFM state is energetically more stable compared to the FM and NM state over a wide range of lattice volumes. This is consistent with the experimental observation that MP-type CrAs is in AFM state³⁹. The equilibrium lattice volume of AFM MP-type CrAs is found to be 31.28 \AA^3 .

Then the calculated total energies versus formula volume for CrAs in six crystal structures are displayed in Figure 2(a). For the MP and NA structures only AFM phases are presented because the NM and FM phases are always higher in total energy (see Figure 2(b)). For the other four structures: RS, CC ZB and WZ, we choose ZB as a representative. The calculated total energies as a function of crystal volume for NM, FM, and AFM states of CrAs in ZB-type structure are plotted in Figure 2(c). As seen in this figure, the total calculation indicates that the FM state is most stable for this structure. This is consistent with the previous work that ZB-type CrAs is an FM state^{19,37}. Thus, only the FM phases of ZB, CC, WZ, RS are presented in Figure 2(a) because the NM and AFM phases are always higher in total energy. The results of structural properties and magnetic moments of six structures for CrAs together with theoretical and experimental results are summarized in Table I.

As seen from Table I, it can be seen that the fully optimized MP-type CrAs in AFM state is lower in energy than any other phases, so it is the ground-state phase, this agrees well with the experimental ground

state, and theoretical structural parameters in this state are in agreement with experimental values⁸. The NA-type CrAs in AFM state is 40 meV higher than MP-type CrAs in the AFM state (see Figure 2(a)). However, the MP-type CrAs in the FM state has a higher energy of 36 meV than MP-type CrAs in the AFM state (see Figure 2(b)). Thus, the energy of MP-type CrAs in the FM state is slightly smaller than the NA-type CrAs in AFM state and is the second-most stable phase. This may explain that the new metastable FM orthorhombic structure CrAs epilayers can be grown on GaAs(001) in a recent experiment⁴⁰, and it also agrees with the results of Hashemifar's³⁹.

The metastable structure with the energy next to that of MP and NA structure is the CC structure (see Figure 2(a)) which prefers an FM state. The ZB-type CrAs, which has been synthesized in the experiment²⁰, is 0.885 eV higher in energy than MP-type AFM state, it agrees well with former's work³⁹. The equilibrium energy and volumes of the FM ZB-type and FM WZ-type are almost the same, with their difference being only 2 meV and 0.09 \AA^3 , respectively.

C. The magnetic properties of CrAs

CrAs in ZB, CC, WZ and, RS phase prefer the FM state. We calculated the magnetic moments of those four structures in the FM phase at different volumes, and the results are presented in Table I and Figure 2(d). The magnetic moment for ZB-type and WZ-type CrAs in FM state was calculated as $3 \mu_B$ per CrAs pair at the equilibrium volumes, which is in excellent agreement with the saturation moments estimated experimentally¹⁹ and theoretical results³⁷. The net moment of $3.0 \mu_B$ results from the remaining four of the 3d plus two of 4s electrons of chromium bonding with the three As p electrons. The magnetic moments of ZB-type and WZ-type

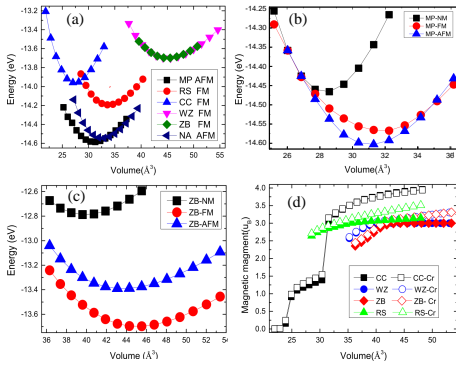


FIG. 2. (a) Total energy as a function of volume for CrAs in six crystal structures. For every structure only the lowest phase of NM, AFM and FM is shown. Energy as a function of volume of CrAs in the NM, FM and AFM states at (b) MP-type and (c) ZB-type structure, respectively. (d) Magnetic moment-volume curves of four crystal structure CrAs in FM state.

CrAs remain unchanged under compressive strain down to -12% and -5% in relative volumes, respectively.

RS-type CrAs has a magnetic moment of $2.9\mu_B$ and $3\mu_B$ per CrAs pair at the equilibrium volumes and expanded volumes, respectively. CC-type CrAs has a magnetic moment of only $1.183\mu_B$ per CrAs pair at the equilibrium volumes. However, the magnetic moments of CC-FM grow rapidly with increasing volume.

D. Electronic properties of CrAs

To study the electronic structures of the system, the density of states (DOS) are calculated with these optimized structures. Spin-resolved DOS of in RS-, CC-, ZB- and WZ-type CrAs in the FM state are presented in Figure 3. The Cr-d orbitals dominated the DOS around the Fermi level.

We defined the E_{bc} and E_{tv} as the bottom energy of minority-spin conduction bands and absolute values of the top energy of minority-spin valance bands with respect to the Fermi energy, respectively. The half-metallic (HM) gap is defined as the minimum of E_{bc} and E_{tv} . In ZB and WZ phases, there are clear non-zero HM gap, which is essential to a half-metallic ferromagnet with 100% spin-polarized carriers. Large HM gaps in WZ-type FM phase reaches 0.49 eV , which agrees well with former's work^{22,37}. For the mechanism of HM in the ZB and WZ structures of CrAs, please see the Ref^{22,37,41}.

Figure 3(c) displayed the DOS of RS-type CrAs. The DOS at minority-spin channel is non zero. The lack of HM gap around the Fermi level indicate that RS-type structure is not HM, but has a high spin polarization. Contrast with RS, ZB, and WZ structures, CC-type CrAs has a small a spin polarization of 2.8% at the Fermi level.

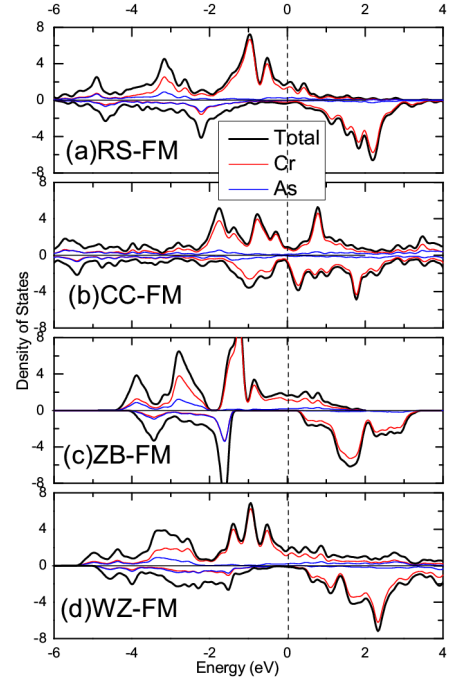


FIG. 3. Spin-dependent total densities of states (DOS, states/eV per formula unit) of the four FM CrAs in stable magnetic state. Upper and lower parts of every panel are for majority-spin and minority-spin, respectively.

E. Optical properties of CrAs

We further calculated the dielectric function to study the optical properties of CrAs. Since the CC-, ZB- and RS- type CrAs have isotropic lattices, only the results for the a-axis are presented. Considering the anisotropy lattice of MP, NA, and WZ structure, the results for the a-axis and c-axis (including b-axis for MP) are displayed.

As shown in Figure 4(a) and 4(b), the absorption coefficient α of NA-type CrAs in the infrared region (0.6 eV - 1.3 eV) is higher than that of other phases along different axis. In the ultraviolet region (3.5 eV - 5 eV), the NA structure has a higher α along the a-axis, and the MP structure has a slightly higher α along the b-axis.

Based on Figure 4(c) and 4(d), it can be seen that NA structure has a higher reflectivity R in the infrared region (0.6 eV - 1.3 eV). The R of NA structure along the c axis is 78.9% at 1.435 eV , which is significantly higher than other phases. In the visible light region (1.64 eV - 3.19 eV), the R of WZ and ZB structures along the a-axis is lower than other phases, and there is no such phenomenon on the c-axis. And the R of NA and MP structures along the a-axis in the ultraviolet region (3.5 eV - 5 eV) is significantly higher than other phases.

The energy loss spectrum L corresponds to the reflection coefficient R , and the position with the largest energy loss corresponds to the position where the reflection coefficient drops sharply. At about 1.8 eV , the reflection

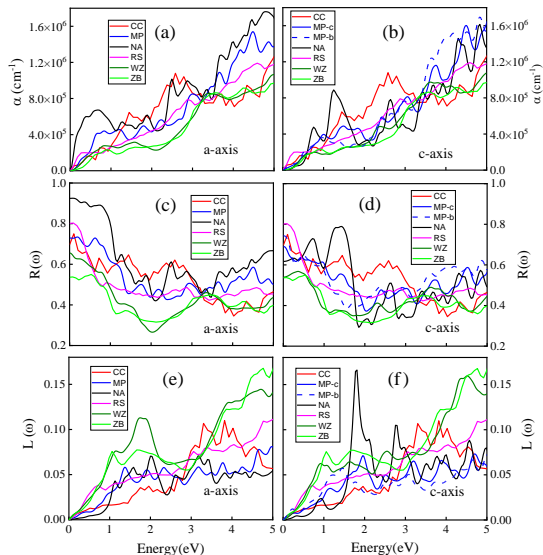


FIG. 4. Spectra of different phases of CrAs in the direction of a-axis and c-axis (including b-axis): (a) and (b) absorption coefficient; (c) and (d) reflectivity; (e) and (f) energy loss spectrum.

curvature of NA structure along the c axis decreases, and the energy loss coefficient has a peak at the same energy position. Similarly, the reflection curve of CC and WZ structures drops about 3.0 eV and 1.8 eV along the a-axis, respectively. As a results, the energy loss coefficient has a peak at the same energy position.

F. Doping effect

At last, we investigated the effect of external doping on the structural and magnetic properties of CrAs.

Firstly, we substituted the Cr atom in CrAs by Ti atom at different doping concentration x . We calculated the energy of the compound $\text{Cr}_{1-x}\text{Ti}_x$ in different structures and different magnetic state. We found that MP and NA structures still have lower energy than other structures. The phase diagram of the CrAs system is shown as the inset of Figure 5 (a), which is drawn based on the energy difference between the MP-type and the NA-type $\Delta E = E_{\text{MP}} - E_{\text{NA}}$. It is found that the ground-state crystal structure is the orthorhombic MP-type when the doping concentration of $x \leq 0.12$. However, the compound $\text{Cr}_{1-x}\text{Ti}_x$ prefers the hexagonal NA-type structure for $x > 0.12$. We have examined the MP-type and NA-type $\text{Cr}_{1-x}\text{Ti}_x$ compound in different magnetic state. The energy-volume curve of $x = 0.125$ at which CrAs exhibit a NA structure. It is shown that the ground-state phase is FM state. The electronic state calculation indicates that Ti-doped CrAs at $x = 0.125$ is a magnetic metal.

Then we considering the substitution of the As atom by Te atom at different doping concentration x . We found

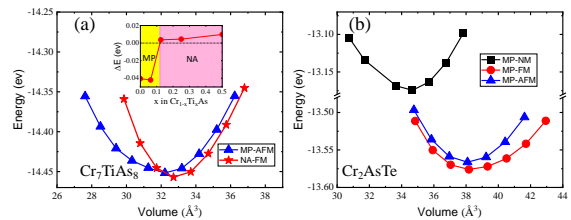


FIG. 5. (a) Total energy as a function of volume for Cr_7TiAs_8 in MP-type and NA-type structure. For every structure only the lowest phase of NM, AFM and FM is shown. The inset presents the difference between the MP-type and NA-type $\Delta E = E_{\text{MP}} - E_{\text{NA}}$ for the $\text{Cr}_{1-x}\text{Ti}_x\text{As}$ system. (b) Total energy as a function of volume for Cr_2AsTe in NM, FM, AFM state at MP-type structure.

that the compound $\text{CrAs}_{1-x}\text{Te}_x$ still maintained the orthogonal MnP-type structure as ground-state structure but has a magnetic phase transition from AFM to FM at $x=0.5$, as shown in Figure 5 (b). The electronic state calculation indicates that Te-doped CrAs at $x = 0.5$ is also a magnetic metal. We noticed that doping concentration in CrAs have reach more than 50 %²⁵, so the structural and magnetic phase transition might be observed in future experiment and be applied in the spintronic devices.

IV. CONCLUSION

We adopted the first-principles calculations to study the structural, magnetic, optical properties, and doping effect in CrAs system with different structures. It was found that the FM state is energetically favorable for RS-type, CC-type, ZB-type, and WZ-type structure, while AFM state is energetically favorable for NA-type and MP-type structure. MP-type structure in AFM state is the ground-state structure for CrAs. The density of states show that ZB-type and WZ-type structures exhibit HM behavior with a band gap in spin-down channel. RS-type and CC-type CrAs is not HM and has a large and small spin-polarization at the Fermi level, respectively. The optical properties show that the NA-type has a higher absorption coefficient and reflectivity in the infrared region at all the axis. NA-type and MP-type have high absorption coefficients and reflectivity in the ultraviolet region along the a-axis. WZ-type and ZB-type have small absorption coefficients in the visible light region. At last, we found that Ti-doped CrAs occur a structural phase transition from MP-type to NA-type structure at a doping concentration of about $x = 0.12$. The Te-doped CrAs can maintain the structure and exhibit an AFM-to-FM phase transition at a doping concentration of about $x = 0.5$. We hope our results can stimulate further interest in both theoretical and experimental research in the binary compound CrAs.

ACKNOWLEDGMENTS

This work was supported by National Natural Science Foundation of China (No. 11904312 and 11904313), the Project of Department of Education of Hebei Province, China (No. BJ2020015), and the Natural Science Foundation of Hebei Province (No. A2019203507 and A2020203027). K.C. Zhang acknowledges the fund support from Liaoning Revitalization Talents Program (No. XLYC2007120). The authors thank the High Performance Computing Center of Yanshan University.

- ¹I. Žutić, J. Fabian, and S. Das Sarma, “Spintronics: Fundamentals and applications,” *Rev. Mod. Phys.* **76**, 323–410 (2004).
- ²G. A. Prinz, “Magnetoelectronics,” *Science* **282**, 1660–1663 (1998).
- ³G. A. Prinz, “Magnetoelectronics applications,” *J. Magn. Magn. Mater.* **200**, 57–68 (1999).
- ⁴S. A. Wolf, D. D. Awschalom, R. A. Buhrman, J. M. Daughton, S. von Molnár, M. L. Roukes, A. Y. Chtchelkanova, and D. M. Treger, “Spintronics: A spin-based electronics vision for the future,” *Science* **294**, 1488–1495 (2001).
- ⁵R. A. de Groot, F. M. Mueller, P. G. v. Engen, and K. H. J. Buschow, “New class of materials: Half-metallic ferromagnets,” *Phys. Rev. Lett.* **50**, 2024–2027 (1983).
- ⁶Z. Charifi, D. Guendouz, H. Baaziz, F. Soyalp, and B. Hamad, “Ab-initio investigations of the structural, electronic, magnetic and mechanical properties of CrX (X = As, Sb, Se, and Te) transition metal pnictides and chalcogenides,” *Phys. Scr.* **94**, 015701 (2018).
- ⁷V. Kanchana, G. Vaitheeswaran, and M. Rajagopalan, “Pressure induced structural and magnetic phase transition in ferromagnetic CrTe,” *J. Magn. Magn. Mater.* **250**, 353–363 (2002).
- ⁸K. Selte, A. Kjekshus, W. Jamison, A. Andresen, J. Engebretsen, and L. Ehrenberg, “Magnetic structure and properties of CrAs,” *Acta Chem. Scand.* **25**, 1703–1714 (1971).
- ⁹H. Watanabe, N. Kazama, Y. Yamaguchi, and M. Ohashi, “Magnetic structure of CrAs and Mn-substituted CrAs,” *J. Appl. Phys.* **40**, 1128–1129 (1969).
- ¹⁰T. Ito, H. Ido, and K. Motizuki, “Electronic structure and magnetic properties in CrX (XP, As and Sb),” *J. Magn. Magn. Mater.* **310**, e558–e559 (2007).
- ¹¹H. Boller and A. Kallel, “First order crystallographic and magnetic phase transition in CrAs,” *Solid State Commun.* **9**, 1699–1706 (1971).
- ¹²S. Polesya, G. Kuhn, D. Benea, S. Mankovsky, and H. Ebert, “Electronic structure and magnetic properties of chromium chalcogenides and pnictides with nias structure,” *Z. Anorg. Allg. Chem.* **639**, 2826–2835 (2013).
- ¹³H. Kotegawa, S. Nakahara, H. Tou, and H. Sugawara, “Superconductivity of 2.2 K under pressure in helimagnet CrAs,” *J. Phys. Soc. Jpn.* **83**, 093702 (2014).
- ¹⁴W. Wu, J. Cheng, K. Matsubayashi, P. Kong, F. Lin, C. Jin, N. Wang, Y. Uwatoko, and J. Luo, “Superconductivity in the vicinity of antiferromagnetic order in CrAs,” *Nat. Commun.* **5**, 5508 (2014).
- ¹⁵H. Kotegawa, S. Nakahara, R. Akamatsu, H. Tou, H. Sugawara, and H. Harima, “Detection of an unconventional superconducting phase in the vicinity of the strong first-order magnetic transition in CrAs using ⁷⁵As-nuclear quadrupole resonance,” *Phys. Rev. Lett.* **114**, 117002 (2015).
- ¹⁶C. Autieri and C. Noce, “First principles study of structural, magnetic and electronic properties of CrAs,” *Philos. Mag.* **97**, 3276–3295 (2017).
- ¹⁷W. Wu, X.-D. Zhang, Z. Yin, P. Zheng, N. Wang, and J. Luo, “Low temperature properties of pnictide CrAs single crystal,” *Sci. China Phys., Mech. Astron.* **53**, 1207–1211 (2010).
- ¹⁸N. Kazama and H. Watanabe, “Magnetic properties of Cr_{1-x}Mn_x as system,” *J. Phys. Soc. Jpn.* **30**, 1319–1329 (1971), <https://doi.org/10.1143/JPSJ.30.1319>.
- ¹⁹H. Akinaga, T. Manago, and M. Shirai, “Material design of half-metallic zinc-blende CrAs and the synthesis by molecular-beam epitaxy,” *Jpn. J. Appl. Phys.* **39**, L1118–L1120 (2000).
- ²⁰H. Ofuchi, M. Mizuguchi, K. Ono, M. Oshima, H. Akinaga, and T. Manago, “Fluorescence extended x-ray absorption fine structure analysis of half-metallic ferromagnet zinc-blende CrAs grown on GaAs by molecular beam epitaxy,” *Nucl. Instrum. Meth.* **199**, 227–230 (2003).
- ²¹M. Shirai, “Possible half-metallic ferromagnetism in zinc blende CrSb and CrAs,” *J. Appl. Phys.* **93**, 6844–6846 (2003).
- ²²W.-H. Xie, B.-G. Liu, and D. G. Pettifor, “Half-metallic ferromagnetism in transition metal pnictides and chalcogenides with wurtzite structure,” *Phys. Rev. B* **68**, 134407 (2003).
- ²³T. Suzuki and H. Ido, “Magnetic-nonmagnetic transition in CrAs and the related compounds,” *J. Appl. Phys.* **73**, 5686–5688 (1993).
- ²⁴K. Selte, H. Hjersing, A. Kjekshus, A. F. Andresen, and P. M. Pedersen, “Magnetic structures and properties of V_{1-t}Cr_tAs,” *Acta Chem. Scand.* **29a**, 312–316 (1975).
- ²⁵H. Ido, N. Hong, O. Nashima, and T. Suzuki, “Weak ferromagnetism in Cr_{1-x}Fe_xAs compound system,” *Physica B* **237-238**, 164–166 (1997).
- ²⁶G. Kresse and J. Furthmüller, “Efficient iterative schemes for ab initio total-energy calculations using a plane-wave basis set,” *Phys. Rev. B* **54**, 11169–11186 (1996).
- ²⁷G. Kresse and J. Furthmüller, “Efficiency of ab-initio total energy calculations for metals and semiconductors using a plane-wave basis set,” *Comput. Mater. Sci.* **6**, 15–50 (1996).
- ²⁸G. Kresse and J. Hafner, “Ab initio molecular-dynamics simulation of the liquid-metal–amorphous-semiconductor transition in germanium,” *Phys. Rev. B* **49**, 14251–14269 (1994).
- ²⁹M. C. Payne, M. P. Teter, D. C. Allan, T. A. Arias, and J. D. Joannopoulos, “Iterative minimization techniques for ab initio total-energy calculations: molecular dynamics and conjugate gradients,” *Rev. Mod. Phys.* **64**, 1045–1097 (1992).
- ³⁰J. P. Perdew, K. Burke, and M. Ernzerhof, “Generalized gradient approximation made simple,” *Phys. Rev. Lett.* **77**, 3865–3868 (1996).
- ³¹H. J. Monkhorst and J. D. Pack, “Special points for brillouin-zone integrations,” *Phys. Rev. B* **13**, 5188–5192 (1976).
- ³²H. Wang, G. Qin, J. Yang, Z. Qin, Y. Yao, Q. Wang, and M. Hu, “First-principles study of electronic, optical and thermal transport properties of group III–VI monolayer MX (M = Ga, In; X = S, Se),” *J. Appl. Phys.* **125**, 245104 (2019).
- ³³Y. Xu, H. Zhang, H. Shao, G. Ni, J. Li, H. Lu, R. Zhang, B. Peng, Y. Zhu, H. Zhu, and C. M. Soukoulis, “First-principles study on the electronic, optical, and transport properties of monolayer α - and β -GeSe,” *Phys. Rev. B* **96**, 245421 (2017).
- ³⁴R. Podloucky, “Electronic structure of CrAs and FeAs,” *J. Magn. Magn. Mater.* **43**, 291–296 (1984).
- ³⁵B. Sagarov, J. E. Mitchell, and A. S. Sefat, “Properties of binary transition-metal arsenides (TAs),” *Supercond. Sci. Technol.* **25**, 084016 (2012).
- ³⁶K. Motizuki, K. Katoh, and A. Yanase, “Electronic band structures of NiAs-type compounds. i. nonmagnetic state,” *J. Phys. C: Solid State Phys.* **19**, 495–509 (1986).
- ³⁷W.-H. Xie, Y.-Q. Xu, B.-G. Liu, and D. G. Pettifor, “Half-metallic ferromagnetism and structural stability of zincblende phases of the transition-metal chalcogenides,” *Phys. Rev. Lett.* **91**, 037204 (2003).
- ³⁸K. Motizuki, H. Ido, T. Itoh, and M. Morifuji, “Electronic structure and magnetism of 3d-transition metal pnictides,” *Mater. Sci.* **131**, 1–132 (2009).
- ³⁹S. J. Hashemifar, P. Kratzer, and M. Scheffler, “Stable structure and magnetic state of ultrathin CrAs films on GaAs(001): A density functional theory study,” *Phys. Rev. B* **82**, 214417 (2010).

⁴⁰V. H. Etgens, P. C. de Camargo, M. Eddrief, R. Mattana, J. M. George, and Y. Garreau, "Structure of ferromagnetic CrAs epilayers grown on GaAs(001)," *Phys. Rev. Lett.* **92**, 167205 (2004).

⁴¹P. Mavropoulos and I. Galanakis, "A review of the electronic and magnetic properties of tetrahedrally bonded half-metallic ferromagnets," *J. Phys.: Condens. Matter* **19**, 315221 (2007).